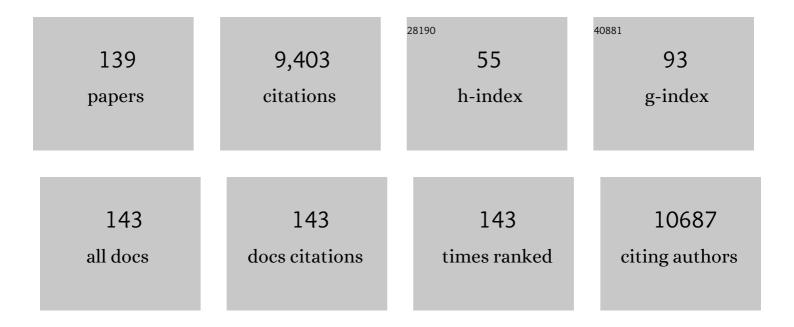
List of Publications by Year in descending order

Source: https://exaly.com/author-pdf/4155527/publications.pdf Version: 2024-02-01



#	Article	IF	CITATIONS
1	Monolayered Bi2WO6 nanosheets mimicking heterojunction interface with open surfaces for photocatalysis. Nature Communications, 2015, 6, 8340.	5.8	578
2	Amine-functionalized zirconium metal–organic framework as efficient visible-light photocatalyst for aerobic organic transformations. Chemical Communications, 2012, 48, 11656.	2.2	405
3	Nitrogen-Doped Graphene Nanosheets as Metal-Free Catalysts for Aerobic Selective Oxidation of Benzylic Alcohols. ACS Catalysis, 2012, 2, 622-631.	5.5	384
4	Visible-Light Driven Overall Conversion of CO ₂ and H ₂ O to CH ₄ and O ₂ on 3D-SiC@2D-MoS ₂ Heterostructure. Journal of the American Chemical Society, 2018, 140, 14595-14598.	6.6	361
5	Photocatalytic reforming of biomass: A systematic study of hydrogen evolution from glucose solution. International Journal of Hydrogen Energy, 2008, 33, 6484-6491.	3.8	301
6	Amorphous NiO as co-catalyst for enhanced visible-light-driven hydrogen generation over g-C 3 N 4 photocatalyst. Applied Catalysis B: Environmental, 2018, 222, 35-43.	10.8	252
7	Efficient and Selective Photocatalytic Oxidation of Benzylic Alcohols with Hybrid Organic–Inorganic Perovskite Materials. ACS Energy Letters, 2018, 3, 755-759.	8.8	222
8	Template-free synthesis of porous graphitic carbon nitride microspheres for enhanced photocatalytic hydrogen generation with high stability. Applied Catalysis B: Environmental, 2015, 165, 503-510.	10.8	207
9	Gold plasmon-induced photocatalytic dehydrogenative coupling of methane to ethane on polar oxide surfaces. Energy and Environmental Science, 2018, 11, 294-298.	15.6	202
10	Nitrogen-doped titanium dioxide visible light photocatalyst: Spectroscopic identification of photoactive centers. Journal of Catalysis, 2010, 276, 201-214.	3.1	185
11	Organic semiconductor for artificial photosynthesis: water splitting into hydrogen by a bioinspired C ₃ N ₃ S ₃ polymer under visible light irradiation. Chemical Science, 2011, 2, 1826-1830.	3.7	167
12	Direct Z-Scheme Heterojunction of Semicoherent FAPbBr ₃ /Bi ₂ WO ₆ Interface for Photoredox Reaction with Large Driving Force. ACS Nano, 2020, 14, 16689-16697.	7.3	167
13	Gold-plasmon enhanced solar-to-hydrogen conversion on the {001} facets of anatase TiO2 nanosheets. Energy and Environmental Science, 2014, 7, 973.	15.6	159
14	Dual couples Bi metal depositing and Ag@AgI islanding on BiOI 3D architectures for synergistic bactericidal mechanism of E. coli under visible light. Applied Catalysis B: Environmental, 2017, 204, 1-10.	10.8	156
15	Bi ₂ MoO ₆ Nanobelts for Crystal Facetâ€Enhanced Photocatalysis. Small, 2014, 10, 2791-2795.	5.2	145
16	One-pot fabrication of Bi3O4Cl/BiOCl plate-on-plate heterojunction with enhanced visible-light photocatalytic activity. Applied Catalysis B: Environmental, 2016, 185, 203-212.	10.8	141
17	Hot Ï€â€Electron Tunneling of Metal–Insulator–COF Nanostructures for Efficient Hydrogen Production. Angewandte Chemie - International Edition, 2019, 58, 18290-18294.	7.2	138
18	Subsurface Defect Engineering in Single-Unit-Cell Bi ₂ WO ₆ Monolayers Boosts Solar-Driven Photocatalytic Performance. ACS Catalysis, 2020, 10, 1439-1443.	5.5	138

#	Article	IF	CITATIONS
19	All-solid-state direct Z-scheme NiTiO ₃ /Cd _{0.5} Zn _{0.5} S heterostructures for photocatalytic hydrogen evolution with visible light. Journal of Materials Chemistry A, 2021, 9, 10270-10276.	5.2	136
20	Layered metal–organic framework/graphene nanoarchitectures for organic photosynthesis under visible light. Journal of Materials Chemistry A, 2015, 3, 24261-24271.	5.2	130
21	In situ IR study of surface hydroxyl species of dehydrated TiO2: towards understanding pivotal surface processes of TiO2 photocatalytic oxidation of toluene. Physical Chemistry Chemical Physics, 2012, 14, 9468.	1.3	127
22	Hydroxide ZnSn(OH)6: A promising new photocatalyst for benzene degradation. Applied Catalysis B: Environmental, 2009, 91, 67-72.	10.8	122
23	C(sp ³)–H Bond Activation by Perovskite Solar Photocatalyst Cell. ACS Energy Letters, 2019, 4, 203-208.	8.8	114
24	Photocatalytic reduction of CO ₂ with H ₂ O to CH ₄ on Cu(<scp>i</scp>) supported TiO ₂ nanosheets with defective {001} facets. Physical Chemistry Chemical Physics, 2015, 17, 9761-9770.	1.3	110
25	Hydrothermal synthesis, characterization, and photocatalytic properties of Zn2SnO4. Journal of Solid State Chemistry, 2009, 182, 517-524.	1.4	108
26	Efficient Photocatalytic Degradation of Volatile Organic Compounds by Porous Indium Hydroxide Nanocrystals. Environmental Science & amp; Technology, 2010, 44, 1380-1385.	4.6	96
27	A Longâ€Lived Mononuclear Cyclopentadienyl Ruthenium Complex Grafted onto Anatase TiO ₂ for Efficient CO ₂ Photoreduction. Angewandte Chemie - International Edition, 2016, 55, 8314-8318.	7.2	96
28	Plasmonic control of solar-driven CO2 conversion at the metal/ZnO interfaces. Applied Catalysis B: Environmental, 2019, 256, 117823.	10.8	95
29	Vacuum heat-treatment of carbon nitride for enhancing photocatalytic hydrogen evolution. Journal of Materials Chemistry A, 2014, 2, 17797-17807.	5.2	94
30	Intimately Contacted Ni2P on CdS Nanorods for Highly Efficient Photocatalytic H2 Evolution: New Phosphidation Route and the Interfacial Separation Mechanism of Charge Carriers. Applied Catalysis B: Environmental, 2021, 281, 119443.	10.8	90
31	Single-site Sn-grafted Ru/TiO2 photocatalysts for biomass reforming: Synergistic effect of dual co-catalysts and molecular mechanism. Journal of Catalysis, 2013, 303, 141-155.	3.1	89
32	Layered C ₃ N ₃ S ₃ Polymer/Graphene Hybrids as Metal-Free Catalysts for Selective Photocatalytic Oxidation of Benzylic Alcohols under Visible Light. ACS Catalysis, 2014, 4, 3302-3306.	5.5	89
33	Amorphous Ta2OxNy-enwrapped TiO2 rutile nanorods for enhanced solar photoelectrochemical water splitting. Applied Catalysis B: Environmental, 2019, 243, 481-489.	10.8	86
34	Cul-BiOl/Cu film for enhanced photo-induced charge separation and visible-light antibacterial activity. Applied Catalysis B: Environmental, 2018, 235, 238-245.	10.8	85
35	Nitrogen-doped graphene stabilized gold nanoparticles for aerobic selective oxidation of benzylic alcohols. RSC Advances, 2012, 2, 12438.	1.7	84
36	Catalytic Role of Cu Sites of Cu/MCM-41 in Phenol Hydroxylation. Langmuir, 2010, 26, 1362-1371.	1.6	80

#	Article	IF	CITATIONS
37	A Longâ€Lived Mononuclear Cyclopentadienyl Ruthenium Complex Grafted onto Anatase TiO ₂ for Efficient CO ₂ Photoreduction. Angewandte Chemie, 2016, 128, 8454-8458.	1.6	80
38	Synthesis of caged iodine-modified ZnO nanomaterials and study on their visible light photocatalytic antibacterial properties. Applied Catalysis B: Environmental, 2019, 256, 117873.	10.8	79
39	Structural evolution of alkaline earth metal stannates MSnO ₃ (M = Ca, Sr, and Ba) photocatalysts for hydrogen production. RSC Advances, 2016, 6, 42474-42481.	1.7	78
40	Integrating single Ni sites into biomimetic networks of covalent organic frameworks for selective photoreduction of CO ₂ . Chemical Science, 2020, 11, 6915-6922.	3.7	78
41	Controlling the synergistic effect of oxygen vacancies and N dopants to enhance photocatalytic activity of N-doped TiO2 by H2 reduction. Applied Catalysis A: General, 2012, 425-426, 117-124.	2.2	76
42	Urea-based hydrothermal growth, optical and photocatalytic properties of single-crystalline In(OH)3 nanocubes. Journal of Colloid and Interface Science, 2008, 325, 425-431.	5.0	75
43	Au deposited BiOCl with different facets: On determination of the facet-induced transfer preference of charge carriers and the different plasmonic activity. Applied Catalysis B: Environmental, 2014, 160-161, 98-105.	10.8	75
44	Highâ€Rate, Tunable Syngas Production with Artificial Photosynthetic Cells. Angewandte Chemie - International Edition, 2019, 58, 7718-7722.	7.2	75
45	Surface Chlorination of TiO ₂ -Based Photocatalysts: A Way to Remarkably Improve Photocatalytic Activity in Both UV and Visible Region. ACS Catalysis, 2011, 1, 200-206.	5.5	71
46	Robust Photocatalytic H2O2 Production by Octahedral Cd3(C3N3S3)2 Coordination Polymer under Visible Light. Scientific Reports, 2015, 5, 16947.	1.6	71
47	Synergy of metal and nonmetal dopants for visible-light photocatalysis: a case-study of Sn and N co-doped TiO ₂ . Physical Chemistry Chemical Physics, 2016, 18, 9636-9644.	1.3	68
48	Single-site nickel-grafted anatase TiO 2 for hydrogen production: Toward understanding the nature of visible-light photocatalysis. Journal of Catalysis, 2014, 320, 147-159.	3.1	67
49	Ternary Pt/SnOx/TiO2 photocatalysts for hydrogen production: consequence of Pt sites for synergy of dual co-catalysts. Physical Chemistry Chemical Physics, 2014, 16, 12521.	1.3	65
50	Sn2+ dopant induced visible-light activity of SnO2 nanoparticles for H2 production. Catalysis Communications, 2011, 16, 215-219.	1.6	64
51	Fabrication of robust M/Ag ₃ PO ₄ (M = Pt, Pd, Au) Schottky-type heterostructures for improved visible-light photocatalysis. RSC Advances, 2014, 4, 37220.	1.7	64
52	Reduced Graphene Oxide admium Sulfide Nanorods Decorated with Silver Nanoparticles for Efficient Photocatalytic Reduction Carbon Dioxide Under Visible Light. ChemCatChem, 2018, 10, 1627-1634.	1.8	63
53	Defect engineering of metal–oxide interface for proximity of photooxidation and photoreduction. Proceedings of the National Academy of Sciences of the United States of America, 2019, 116, 10232-10237.	3.3	63
54	lodine-modified nanocrystalline titania for photo-catalytic antibacterial application under visible light illumination. Applied Catalysis B: Environmental, 2015, 176-177, 36-43.	10.8	62

#	Article	IF	CITATIONS
55	Smallâ€Sized Bimetallic CuPd Nanoclusters Encapsulated Inside Cavity of NH ₂ â€UiOâ€66(Zr) with Superior Performance for Lightâ€Induced Suzuki Coupling Reaction. Small Methods, 2018, 2, 1800164.	4.6	59
56	Crystalline Covalent Organic Frameworks with Tailored Linkages for Photocatalytic H ₂ Evolution. ChemSusChem, 2021, 14, 4958-4972.	3.6	56
57	Indium hydroxide: A highly active and low deactivated catalyst for photoinduced oxidation of benzene. Comptes Rendus Chimie, 2008, 11, 101-106.	0.2	55
58	Cd3(C3N3S3)2 coordination polymer/graphene nanoarchitectures for enhanced photocatalytic H2O2 production under visible light. Science Bulletin, 2017, 62, 610-618.	4.3	55
59	Photocatalytic and antibacterial properties of medicalâ€grade PVC material coated with TiO ₂ film. Journal of Biomedical Materials Research - Part B Applied Biomaterials, 2008, 87B, 425-431.	1.6	54
60	Single-site tin-grafted anatase TiO2 for photocatalytic hydrogen production: Toward understanding the nature of interfacial molecular junctions formed in semiconducting composite photocatalysts. Journal of Catalysis, 2012, 289, 88-99.	3.1	49
61	3D flower-like heterostructured TiO2@Ni(OH)2 microspheres for solar photocatalytic hydrogen production. Chinese Journal of Catalysis, 2019, 40, 320-325.	6.9	49
62	Hydrothermal synthesis of MSn(OH)6 (M = Co, Cu, Fe, Mg, Mn, Zn) and their photocatalytic activity for the destruction of gaseous benzene. Chemical Engineering Journal, 2015, 269, 168-179.	6.6	45
63	Visible light-driven decomposition of gaseous benzene on robust Sn ²⁺ -doped anatase TiO ₂ nanoparticles. RSC Advances, 2014, 4, 34315-34324.	1.7	44
64	Reconstructing Dualâ€Induced {0 0 1} Facets Bismuth Oxychloride Nanosheets Heterostructures: An Effective Strategy to Promote Photocatalytic Oxygen Evolution. Solar Rrl, 2019, 3, 1900059.	3.1	44
65	Compact carbon nitride based copolymer films with controllable thickness for photoelectrochemical water splitting. Journal of Materials Chemistry A, 2017, 5, 19062-19071.	5.2	43
66	Photochemical synthesis of submicron- and nano-scale Cu2O particles. Journal of Colloid and Interface Science, 2009, 333, 791-799.	5.0	41
67	Heterogeneous Photocatalyzed Câ^'C Crossâ€coupling Reactions Under Visibleâ€light and Nearâ€infrared Light Irradiation. ChemCatChem, 2019, 11, 669-683.	1.8	41
68	Controlled preparation of In2O3, InOOH and In(OH)3via a one-pot aqueous solvothermal route. New Journal of Chemistry, 2008, 32, 1843.	1.4	39
69	Freestanding N-doped graphene membrane electrode with interconnected porous architecture for efficient capacitive deionization. Carbon, 2022, 187, 86-96.	5.4	39
70	The Holeâ€Tunneling Heterojunction of Hematiteâ€Based Photoanodes Accelerates Photosynthetic Reaction. Angewandte Chemie - International Edition, 2021, 60, 16009-16018.	7.2	37
71	Alkaline-Earth Metals-Doped Pyrochlore Gd2Zr2O7 as Oxygen Conductors for Improved NO2 Sensing Performance. Scientific Reports, 2017, 7, 4684.	1.6	36
72	Heteroatomic Ni, Sn Clusters-Grafted Anatase TiO ₂ Photocatalysts: Structure, Electron Delocalization, and Synergy for Solar Hydrogen Production. Journal of Physical Chemistry C, 2015, 119, 10478-10492.	1.5	35

#	Article	IF	CITATIONS
73	Activation of Carbonyl Oxygen Sites in βâ€Ketoenamineâ€Linked Covalent Organic Frameworks via Cyano Conjugation for Efficient Photocatalytic Hydrogen Evolution. Small, 2021, 17, e2101017.	5.2	34
74	Controlled synthesis of pure and highly dispersive Cu(ii), Cu(i), and Cu(0)/MCM-41 with Cu[OCHMeCH2NMe2]2/MCM-41 as precursor. New Journal of Chemistry, 2009, 33, 2044.	1.4	33
75	Electricâ€Fieldâ€Mediated Electron Tunneling of Supramolecular Naphthalimide Nanostructures for Biomimetic H ₂ Production. Angewandte Chemie - International Edition, 2021, 60, 1235-1243.	7.2	33
76	Siteâ€Sensitive Selective CO ₂ Photoreduction to CO over Gold Nanoparticles. Angewandte Chemie - International Edition, 2022, 61, e202204563.	7.2	33
77	Hot Ï€â€Electron Tunneling of Metal–Insulator–COF Nanostructures for Efficient Hydrogen Production. Angewandte Chemie, 2019, 131, 18458-18462.	1.6	31
78	Molecular Dipoleâ€Induced Photoredox Catalysis for Hydrogen Evolution over Selfâ€Assembled Naphthalimide Nanoribbons. Angewandte Chemie - International Edition, 2022, 61, .	7.2	31
79	Highly Efficient Plasmon Induced Hot-Electron Transfer at Ag/TiO ₂ Interface. ACS Photonics, 2021, 8, 1497-1504.	3.2	30
80	Solar Photocatalytic Oxidation of Methane to Methanol with Water over RuO _{<i>x</i>} /ZnO/CeO ₂ Nanorods. ACS Sustainable Chemistry and Engineering, 2022, 10, 16-22.	3.2	30
81	Probing the Electronic Structure and Photoactivation Process of Nitrogenâ€Đoped TiO ₂ Using DRS, PL, and EPR. ChemPhysChem, 2012, 13, 1542-1550.	1.0	29
82	Gold Plasmonâ€Enhanced Solar Hydrogen Production over SrTiO ₃ /TiO ₂ Heterostructures. ChemCatChem, 2019, 11, 6203-6207.	1.8	29
83	Metallic Pt and PtO ₂ Dual-Cocatalyst-Loaded Binary Composite RGO-CN <i>_x</i> for the Photocatalytic Production of Hydrogen and Hydrogen Peroxide. ACS Sustainable Chemistry and Engineering, 2021, 9, 6380-6389.	3.2	29
84	Low-crystalline PdCu alloy on large-area ultrathin 2D carbon nitride nanosheets for efficient photocatalytic Suzuki coupling. Applied Catalysis B: Environmental, 2022, 300, 120756.	10.8	29
85	Plasma-assisted in-situ preparation of graphene-Ag nanofiltration membranes for efficient removal of heavy metal ions. Journal of Hazardous Materials, 2022, 423, 127012.	6.5	29
86	Infrared Study of the NO Reduction by Hydrocarbons over Iron Sites with Low Nuclearity: Some New Insight into the Reaction Pathway. Journal of Physical Chemistry C, 2010, 114, 15713-15727.	1.5	28
87	Molecular p–n heterojunction-enhanced visible-light hydrogen evolution over a N-doped TiO ₂ photocatalyst. Catalysis Science and Technology, 2017, 7, 2039-2049.	2.1	27
88	Graphitic carbon/carbon nitride hybrid as metal-free photocatalyst for enhancing hydrogen evolution. Applied Catalysis A: General, 2017, 546, 30-35.	2.2	27
89	Self-assembled micro/nano-structured Zn2GeO4 hollow spheres: direct synthesis and enhanced photocatalytic activity. Journal of Materials Chemistry A, 2013, 1, 10622.	5.2	26
90	I-TiO2/PVC film with highly photocatalytic antibacterial activity under visible light. Colloids and Surfaces B: Biointerfaces, 2016, 144, 196-202.	2.5	26

#	Article	IF	CITATIONS
91	Molecular Engineering of Fully Conjugated sp ² Carbonâ€Linked Polymers for Highâ€Efficiency Photocatalytic Hydrogen Evolution. ChemSusChem, 2020, 13, 672-676.	3.6	26
92	Ce incorporated pyrochlore Pr2Zr2O7 solid electrolytes for enhanced mild-temperature NO2 sensing. Ceramics International, 2017, 43, 11799-11806.	2.3	24
93	A graphene-hidden structure with diminished light shielding effect: more efficient graphene-involved composite photocatalysts. Catalysis Science and Technology, 2018, 8, 4734-4740.	2.1	24
94	A Mononuclear Cyclopentadiene–Iron Complex Grafted in the Supercages of HY Zeolite: Synthesis, Structure, and Reactivity. Chemistry - A European Journal, 2007, 13, 7890-7899.	1.7	23
95	Binuclear μ-hydroxo-bridged iron clusters derived from surface organometallic chemistry of ferrocene in cavities of HY zeolite: Local structure, bound sites, and catalytic reactivity. Journal of Catalysis, 2009, 264, 163-174.	3.1	23
96	Visible-light photocatalytic denitrogenation of nitrogen-containing compound in petroleum by metastable Bi20TiO32. International Journal of Hydrogen Energy, 2014, 39, 13401-13407.	3.8	23
97	Pyrochlore Pr2Zr2-xMxO7+δ (M =â€Al, Ga, In) solid-state electrolytes: Defect-mediated oxygen hopping pathways and enhanced NO2 sensing properties. Sensors and Actuators B: Chemical, 2018, 270, 130-139.	4.0	23
98	Z-Schemed WO3/rGO/SnIn4S8 Sandwich Nanohybrids for Efficient Visible Light Photocatalytic Water Purification. Catalysts, 2019, 9, 187.	1.6	23
99	Optofluidic Tunable Lenses for In-Plane Light Manipulation. Micromachines, 2018, 9, 97.	1.4	22
100	Understanding structure-function relationships in HZSM-5 zeolite catalysts for photocatalytic oxidation of isopropyl alcohol. Journal of Catalysis, 2019, 377, 322-331.	3.1	21
101	Conversion of CO2 to formic acid by integrated all-solar-driven artificial photosynthetic system. Journal of Power Sources, 2021, 512, 230532.	4.0	21
102	Cyclopentadiene transformation over H-form zeolites: TPD and IR studies of the formation of a monomeric cyclopentenyl carbenium ion intermediate and its role in acid-catalyzed conversions. Journal of Catalysis, 2008, 255, 48-58.	3.1	20
103	One-step synthesis of mesoporous Pt–Nb ₂ O ₅ nanocomposites with enhanced photocatalytic hydrogen production activity. RSC Advances, 2016, 6, 96809-96815.	1.7	20
104	Large-scale preparation of heterometallic chalcogenide MnSb ₂ S ₄ monolayer nanosheets with a high visible-light photocatalytic activity for H ₂ evolution. Chemical Communications, 2016, 52, 13381-13384.	2.2	18
105	Deposition Chemistry of Cu[OCH(Me)CH ₂ NMe ₂] ₂ over Mesoporous Silica. Chemistry of Materials, 2008, 20, 4565-4575.	3.2	16
106	Trinuclear iron cluster intercalated montmorillonite catalyst: Microstructure and photo-Fenton performance. Catalysis Today, 2011, 175, 362-369.	2.2	16
107	Pyrochlore Pr2Zr1.95In0.05O7+δ oxygen conductors: Defect-induced electron transport and enhanced NO2 sensing performances. Electrochimica Acta, 2019, 293, 338-347.	2.6	16
108	Tunable linear donor–π–acceptor conjugated polymers with a vinylene linkage for visible-light driven hydrogen evolution. Catalysis Science and Technology, 2021, 11, 4021-4025.	2.1	16

#	Article	IF	CITATIONS
109	Construction of highly dispersed mononuclear iron-oxo species in the supercages of Y zeolite by use of surface organometallic chemistry. Microporous and Mesoporous Materials, 2008, 108, 258-265.	2.2	15
110	Towards a comprehensive insight into efficient hydrogen production by self-assembled Ru(bpy) ₃ ²⁺ –polymer–Pt artificial photosystems. Physical Chemistry Chemical Physics, 2015, 17, 10726-10736.	1.3	15
111	One-step green conversion of benzyl bromide to aldehydes on NaOH-modified g-C ₃ N ₄ with dioxygen under LED visible light. Catalysis Science and Technology, 2019, 9, 3270-3278.	2.1	15
112	Efficient Photothermal CO2 Methanation over RuO2/SrTiO3. Trends in Chemistry, 2019, 1, 459-460.	4.4	13
113	Tuning Intermediate-Band Cu ₃ VS ₄ Nanocrystals from Plasmonic-like to Excitonic via Shell-Coating. Chemistry of Materials, 2020, 32, 224-233.	3.2	13
114	Photoinduced Reactions between Pb ₃ O ₄ and Organic Dyes in Aqueous Solution under Visible Light. Inorganic Chemistry, 2012, 51, 12594-12596.	1.9	12
115	Highâ€Rate, Tunable Syngas Production with Artificial Photosynthetic Cells. Angewandte Chemie, 2019, 131, 7800-7804.	1.6	12
116	Plasmonic Electronsâ€Driven Solarâ€ŧoâ€Hydrocarbon Conversion over Au NR@ZnO Coreâ€5hell Nanostructures. ChemCatChem, 2020, 12, 2989-2994.	1.8	12
117	Enhanced Hydrogen Production over C-Doped CdO Photocatalyst in NaS/NaSO Solution under Visible Light Irradiation. International Journal of Photoenergy, 2012, 2012, 1-7.	1.4	11
118	Enhanced bacterial disinfection by Cul–BiOI/rGO hydrogel under visible light irradiation. RSC Advances, 2021, 11, 20446-20456.	1.7	11
119	Insight into Photoactive Sites for the Ethylene Oxidation on Commercial HZSM-5 Zeolites with Iron Impurities by UV Raman, X-ray Absorption Fine Structure, and Electron Paramagnetic Resonance Spectroscopies. Journal of Physical Chemistry C, 2007, 111, 5195-5202.	1.5	10
120	<i>In situ</i> construction of layered graphene-based nanofiltration membranes with interlayer photocatalytic purification function and their application for water treatment. Environmental Science: Nano, 2019, 6, 2195-2202.	2.2	10
121	Solar-to-Chemical Fuel Conversion via Metal Halide Perovskite Solar-Driven Electrocatalysis. Journal of Physical Chemistry Letters, 2022, 13, 25-41.	2.1	10
122	Lamellar MXene Nanofiltration Membranes for Electrostatic Modulation of Molecular Permeation: Implications for Fine Separation. ACS Applied Nano Materials, 2022, 5, 7373-7381.	2.4	9
123	H2–O2 promoting effect on photocatalytic degradation of organic pollutants in an aqueous solution without an external H2 supply. Applied Catalysis A: General, 2010, 380, 178-184.	2.2	8
124	Visible light-induced highly efficient organic pollutant degradation and concomitant CO2 fixation using red lead. RSC Advances, 2012, 2, 12624.	1.7	8
125	Interim Anatase Coating Layer Stabilizes Rutile@Cr _{<i>x</i>} O _{<i>y</i>} Photoanode for Visibleâ€Lightâ€Driven Water Oxidation. ChemPhysChem, 2015, 16, 1352-1355.	1.0	8
126	Green synthesis of red-emission carbon based dots by microbial fermentation. New Journal of Chemistry, 2018, 42, 8591-8595.	1.4	8

#	Article	IF	CITATIONS
127	Photoactive sites in commercial HZSM-5 zeolite with iron impurities: An UV Raman study. Comptes Rendus Chimie, 2008, 11, 114-119.	0.2	7
128	Post-synthetic regulation of the structure, morphology and photoactivity of graphitic carbon nitride by heat-vacuum treatment. Materials and Design, 2017, 114, 208-213.	3.3	7
129	Reducing the barrier effect of graphene sheets on a Ag cocatalyst to further improve the photocatalytic performance of TiO ₂ . RSC Advances, 2018, 8, 14056-14063.	1.7	7
130	Molecular Dipoleâ€Induced Photoredox Catalysis for Hydrogen Evolution over Selfâ€Assembled Naphthalimide Nanoribbons. Angewandte Chemie, 2022, 134, .	1.6	7
131	Electricâ€Fieldâ€Mediated Electron Tunneling of Supramolecular Naphthalimide Nanostructures for Biomimetic H 2 Production. Angewandte Chemie, 2021, 133, 1255-1263.	1.6	6
132	Super-hydrophobic and photocatalytic antimicrobial activity of iodine-doped ZnO nanoarray films. New Journal of Chemistry, 2022, 46, 3140-3145.	1.4	6
133	In-situ Formed Surface Complexes Promoting NIR-Light-Driven Carbonylation of Diamine with CO on Ultrathin Co2CO3(OH)2 Nanosheets. Applied Catalysis B: Environmental, 2022, 306, 121103.	10.8	6
134	Site‣ensitive Selective CO ₂ Photoreduction to CO over Gold Nanoparticles. Angewandte Chemie, 2022, 134, .	1.6	5
135	Metal-Free Photocatalysts C ₃ N ₃ S ₃ and its Polymers: Solubility in Water and Application in Benzylic Alcohols Oxidation Under Visible Light. Nano, 2017, 12, 1750101.	0.5	3
136	The Holeâ€Tunneling Heterojunction of Hematiteâ€Based Photoanodes Accelerates Photosynthetic Reaction. Angewandte Chemie, 2021, 133, 16145-16154.	1.6	2
137	Q-switching Yb^3+: YAG lasers based on plasmon resonance nonlinearities of Cu_2â^'xSe@Cu_2â^'xS nanorods. Optics Letters, 2017, 42, 2619.	1.7	1
138	AuPd nanoparticle-decorated ultrathin Bi ₂ TiO ₄ F ₂ sheets for photocatalytic methane oxidation. New Journal of Chemistry, 2022, 46, 10545-10549.	1.4	1
139	Photoelectrochemical reduction of carbon dioxide. , 2021, , 197-210.		Ο